Biomaterials 33 (2012) 4013–4021

Contents lists available at SciVerse ScienceDirect

Biomaterials

journal homepage: www.elsevier.com/locate/biomaterials

The role of the lateral dimension of graphene oxide in the regulation of cellular responses

Hua Yue [a,b,1], Wei Wei [a,1], Zhanguo Yue [a,b], Bin Wang [a], Nana Luo [a,b], Yongjun Gao [c], Ding Ma [c], Guanghui Ma [a,*], Zhiguo Su [a,*]

[a] National Key Laboratory of Biochemical Engineering, Institute of Process Engineering, Chinese Academy of Sciences, P.O. Box 353, Beijing 100190, PR China
[b] Graduate University of the Chinese Academy of Sciences, Beijing 100049, PR China
[c] College of Chemistry and Molecular Engineering, Peking University, Beijing 100871, PR China

ARTICLE INFO

Article history:
Received 29 November 2011
Accepted 7 February 2012
Available online 28 February 2012

Keywords:
Carbon
Cytokine
Cytotoxicity
Drug delivery
Inflammation

ABSTRACT

The nanomaterial graphene oxide (GO) has attracted explosive interests in various areas. However, its performance in biological environments is still largely unknown, particularly with regard to cellular response to GO. Here we separated the GO sheets in different size and systematically investigated size effect of the GO in response to different types of cells. In terms of abilities to internalize GO, enormous discrepancies were observed in the six cell types, with only two phagocytes were found to be capable of internalizing GO. The 2 μm and 350 nm GO greatly differed in lateral dimensions, but equally contributed to the uptake amount in macrophages. Similar amounts of antibody opsonization and active Fcγ receptor-mediated phagocytosis were demonstrated the cause of this behavior. In comparison with the nanosized GO, the GO in micro-size showed divergent intracellular locations and induced much stronger inflammation responses. Present study provided insight into selective internalization, size-independent uptake, and several other biological behaviors undergone by GO. These findings might help build necessary knowledge for potential incorporation of the unique two-dimensional nanomaterial as a biomedical tool, and for avoiding potential hazards.

1. Introduction

Understanding the performance of engineered micro/nano materials in a biological context is an important issue for guiding their biomedical applications. Typically, zero-dimensional (0D) fullerenes and one-dimensional (1D) carbon nanotubes (CNTs) initiated two surges, and the evaluation of their interaction with living matter strongly voted great potentials in cancer therapy, molecular imaging, and drug delivery [1–3]. Following fullerene and CNTs, ultrathin but very strong two-dimensional (2D) graphenes soon draw much more attentions [4–6] and have merited the 2010 Nobel Prize in physics. Apart from the tremendous interest in electrical applications, graphene-based material is also an exciting candidate for exploration in the biological context. The unique 2D high surface area structure can potentially act as a template for cargo molecules (*e.g.* proteins, nucleic acids, and drug entities) [7]. Water-insoluble anti-cancer drugs (*e.g.* hydroxycamptothecin and paclitaxel) are readily adsorbed *via* strong hydrophobic and π-stacking interactions [8], providing a novel strategy for efficient delivery. Small biological or chemical molecules can potentially be inserted between graphene sheets [9], which will further expand its range of uses. Albeit promising, native graphene is subject to poor solubility and high aggregation, which has hampered its biological application. The functionalization of graphene has therefore been exploited, and graphene oxide (GO) is becoming a favored form [10,11], which can be adequately dispersed in water, and allows further functionalization because of its carboxylic groups.

With the immense potential of GO in a very broad future, it is essential to investigate its interaction with cell types that are populous in the body (*e.g.* blood cells) and likely to interact with foreign materials [12–14]. Generally, phagocytes (*e.g.* macrophages) and non-phagocytic cells (*e.g.* endothelial and tumor cells) are the two major cell types involved in biological response to exogenous GO. While macrophages are playing a key role in the non-specific defense (*via* active phagocytosis or cytokines release), non-phagocytic cells are often correlated with tissue impairments and cancerous diseases. Regarding the potential of GO, a number of groups devoted their efforts to GO-based materials in drug delivery (to tumor tissues), photo-thermal therapy, and gene delivery [8,15–17]. These pilot

* Corresponding authors. Tel./fax: +86 10 82627072.
E-mail addresses: ghma@home.ipe.ac.cn (G. Ma), zgsu@home.ipe.ac.cn (Z. Su).
[1] Both authors contributed equally to this work.

0142-9612/$ – see front matter © 2012 Elsevier Ltd. All rights reserved.
doi:10.1016/j.biomaterials.2012.02.021

studies provided impetus on targeted therapeutic as well as diagnostic platforms. However, detailed information about cellular responses to the exogenous GO is still unavailable, which not only hinders the fabrication of graphene-based nano-devices but also delays biological approaches for mechanistic studies.

It has been accepted that the physicochemical properties, especially with aspect to size, can regulate cellular responses to materials, and relevant information is invaluable for their design in biomedical area [18–20]. Material size is known to influence the cellular internalization, which in turn dictates the microenvironments that nanomaterials experience. Therefore, tuning the size of engineered biomaterials is accessible to achieve high cells, tissues, or even subcellular organelles targeting. Unfortunately, how the size of GO with novel 2D structure (with nanometer scale thickness) affects cellular response is poorly understood, which needs to be addressed urgently. In order to fill this knowledge gap, we systematically investigated the effects of GO lateral dimension, from nano to micro, on a series of cellular responses including the cellular uptake, internalization mechanisms, intracellular trafficking, and inflammation response. Two macrophages (peritoneal macrophage PMØ and murine macrophage J774A.1 cell line) and four non-phagocytic cells (murine Lewis lung carcinoma LLC, human breast cancer MCF-7, human hepatocarcinoma cells HepG2, and human umbilical vein endothelial cells HUVEC) were exposed to GO with different lateral dimensions, and the cellular responses were testified by exploring the intrinsic properties of this nanomaterial.

2. Materials and methods

2.1. Materials

Ethylenediaminetetraacetic acid (EDTA), nocodazole, and latrunculin B were purchased from Merck. Glutaradehyde was from Sigma–Aldrich Inc. Penicillin and streptomycin, Gibco Dulbecco's Phosphate-Buffered Saline (D-PBS), Hank's solution, Gibco Dulbecco's Modified Eagle's Medium (DMEM), Rhodamine-phalloidin, 4, 6-diamidino-2-phenylindole (DAPI), Lyso Tracker Red DND-99, and LIVE/DEAD Cell Viability Kit were all bought from Invitrogen. Fetal bovine serum (FBS) was from HyClone. Cell-Counting Kit-8 (CCK8) kit was from the Dojindo Laboratories. BD™ Cytometric Bead Array (CBA) Mouse Inflammation Kit was obtained from BD Biosciences. Mouse Immunology G (Ig G), anti-FcγRI (anti-CD64) antibody (Ab), anti-FcγRIII (anti-CD16) Ab, and anti-mannose receptor (anti-CD206) Ab were ordered from Biolegend. Bovine IgG and horseradish peroxidase (HRP)-labeled Goat Anti-bovine IgG were from KPL Inc. All other reagents were of analytic grade.

2.2. Synthesis and characterization of GO

2.2.1. GO preparation

Preparation of uniform-sized sheets was started from the primary GO that made by a modified Hummers method. After sufficient sonication and washing, the GO sheets were separated by making use of specific sedimentation rates of graphene in different size. The centrifugal forces were selected as 100–200 g and 10,000–30,000 g to obtain the 2 μm GO and 350 nm sheets, respectively. For preparation of Mn-free GO, 3% H_2O_2 solution was used to reduce residual $KMnO_4$ and MnO_2. The solid product was separated by filtration, washed repeatedly with 5% HCl solution until the sulfate could not be detected with $BaCl_2$, and finally washed with deionized water to neutrality.

2.2.2. Atomic force microscopy (AFM) analysis of GO

In virtue of a typical absorption peak at 230 nm induced by the $\pi-\pi^*$ transition of GO [21], concentrations were determined using an Ultrospec 2100 pro UV/Visible spectrophotometer. GO characterization was performed on a BioScope Catalyst AFM (Veeco), operating in tapping mode in air at room temperature.

2.2.3. GO stability and dispersion capacity

To examine the stability and dispersion capacity of GO with the two sizes, 100 μg GO were added to 1 mL water, cell growth medium (DMEM supplemented with 10% FBS) or 100% FBS. Following 6 h incubation, the photos of GO that dispersed in different solutions were captured by using a Canon camera.

2.2.4. Assay of carboxyl groups on GO surface

To detect the carboxyl groups of different GO, we employed a convenient conductometric titration method as described by Hen [22]. In brief, a total quality of 1.5 mg 350 nm GO or 2 μm GO were tittered by a conductometric meter. The surface carboxyl intensity (μmol/g) was calculated by the following equation. Carboxyl groups intensity $= 10^6 \times M \times (V_2 - V_1)/1000/W$ (μmol/g), where M (mol/L) is the concentration of sodium hydroxide (NaOH), $(V_2 - V_1)$ (mL) is the linear fitting volume of NaOH, and W (g) is the GO quality.

2.3. Animals and cells

C57BL/6 male mice (6–8 weeks) were purchased from the National Institute for the Control of Pharmaceutical and Biological Products. All animal experiments were in compliance with the Institutional Ethical Committee for animal care guidelines. PMØ were harvested from the stimulated C57BL/6 mice referring to a typical protocol [23]. All tested cell lines, including J774A.1, LLC, MCF-7, HepG2, and HUVEC, were supplied from ATCC (American Type Culture Collection). These cells were maintained in DMEM supplemented with 10% (v/v) FBS, 100 U/mL penicillin, and 100 g/mL streptomycin. J774A.1 cells were detached by TE (Tris–EDTA), while other cells were detached following usual trypsinization procedure. All cells were grown in a humidified incubator at 37 °C, 5% CO_2.

2.4. Cytotoxicity test of GO sheets

A CCK8 assay was applied to examine the effect of GO on cell viability. Typically, 5000 cells were cultured in each well (100 μL) of 96-well plate and allowed to adhere for 12 h, and then 10 μL serial dilutions of Mn-free or Mn-containing GO (ranging from 0 to 20 μg/mL) were added to the culture medium. After 48 h coincubation, cell samples were treated with 10 μL CCK8 for 1 h at 37 °C. To avoid interference from the residual GO [12], 80 μL supernatants of all tested samples were transferred to a new 96-well plate before the final absorbance measurement. In addition, we prepared wells for background absorbance measurement that containing all material except cells. The water-soluble formazan product, generated by cellular dehydrogenase activity, was determined on an Infinite M200 microplate spectrophotometer (Tecan) at 450 nm. The absorbance was normalized to comparison with the GO-untreated control. For further confirmation, cells were cultured with 10 μg/mL different treated GO sheets for 48 h, and then the cell viability was detected by a LIVE/DEAD Cell Viability Kit according to the manufacture's instruction. Cells without GO treatment were used as control. In this kit, calcein acetoxymethyl ester is cleaved by esterase in live cells to yield green fluorescence, and ethidium homodimer-1 (EthD-1) labels nucleic acids of membrane-compromised cells with red fluorescence. Before analyzing, cell suspensions were filtered through a steel sieve with a quadratic pore size of 50 μm. Finally, 15,000 cells in each sample were analyzed by a CyAn ADP 9 color flow cytometry (FACS, Beckman Coulter).

2.5. GO internalization evaluation in different cell types

Mn-free GO with different diameters were added to the above six cell culture medium at a desired concentration. After a desired period of cultivation, cells were extensively washed, detached, and fixed in 3.7% paraformaldehyde (pH 7.4). The GO internalization was tested using FACS *via* PE-Cy7 channel, and data were acquired from 15,000 cells per sample.

To evaluate the role of receptor-mediated phagocytosis and some important factors on GO internalization, PMØ were pretreated with specific inhibitors for 1 h, which was followed by another 24 h coincubation in the presence of GO. The three receptor-mediated phagocytic pathways were correspondingly blocked by specific chemical inhibitor or antibody. Nocodazole (200 ng/mL) and latrunculin B (0.1 μM) were used to block actin remolding and microtubule movement. The energy-dependent for taking up GO sheets was measured by cultivating cells at low temperature condition (4 °C). In present experiments, the GO internalization at regular 37 °C condition without any pretreatment was used as control.

2.6. Protein adsorption profiles of GO in cell growth medium

Protein adsorption study was carried out according to previous reports [24,25]. In brief, 100 μg GO with different size were added separately to the cell growth medium (10% FBS supplemented DMED) and produced a final concentration of 500 μg GO/mL medium in Eppendorf tubes (2 mL). After 6 h incubation, the samples were centrifuged (10,000 g, 5 min) to remove the unabsorbed protein. GO sediment was resuspended in 1 mL PBS (pH 7.4), washed three times, and then transferred to a new tube prior to the last wash. Proteins were desorbed from GO by 20 min sonication in 200 μL Laemli buffer, followed by a protein denaturation process in 98 °C for 5 min. The samples were subjected to a final quick centrifugation step, and the supernatants were collected and stored at −20 °C before further analysis. Absorbed proteins associated with GO were separated by SDS polyacrylamide gel electrophoresis (SDS-PAGE). As control, 10 μL cell growth medium and 2 μg IgG were used. Gels were detected by a Coomassie Blue staining method or blotted onto a PVDF membrane and stained with anti-bovine IgG-HRP.

2.7. Laser scanning confocal microscopy (CLSM) imaging of internalized GO

To visualize the internalized GO, we seeded PMØ (at a concentration of 2×10^5/mL) in petri dish and exposed them to GO (4 μg/mL) with different size. After a desired

cell-GO interaction period, cells were washed with PBS and fixed in 3.7% paraformaldehyde for 30 min. Cell membranes were subsequently stained with Rhodamine-phalloidin, and corresponding images were obtained by using a TCS SP5 CLSM (Leica). To observe the intracellular location of GO, cell lysosomes were labeled by Lyso Tracker Red DND-99.

2.8. Transmission electron microscopy (TEM) observation of GO-cell interaction

PMØ were allowed to adhere for 24 h in 6-well plates, and GO in different size were added. Following 24 h incubation, cells were rinsed, detached, and then fixed in 2.5% glutaraldehyde (pH 7.4) for 1 h at room temperature. Afterward, samples were post-fixed, serially dehydrated with ethanol, and embedded in Epon. Finally, serial sections were cut on a Reichert Ultracut microtome (Leica), and electron micrographs were taken using a JEM-1400 (JEOL) TEM.

2.9. Cytokine assay of GO stimulated cells

In order to address the size effect of GO on cytokine profile of macrophages, a CBA Mouse Inflammation Kit was employed. PMØ were seeded in 24-well cell culture plates and stimulated with the 350 nm and 2 μm GO for different time (24 h, 48 h, and 96 h) or different dosage (2 μg/mL, 4 μg/mL, and 6 μg/mL). According to the manufacturer's instructions, cell supernatants were collected, and the secretion levels of inflammation cytokines, including IL-6, IL-10, IL-12, TNF-α, MCP-1, and IFN-γ, were detected by using FACS technique. All the plot data were analyzed with the respective BD CBA Analysis Software.

2.10. Measurement of inflammation response to the GO-injection

Mice were separated randomly ($n = 5$) and injected subcutaneously in the neck region with the 350 nm and 2 μm GO at series concentrations. Mice without any treatment were used as control. After 21 day post-injection, mice were sacrificed, and the neck tissues were harvested, fixed in 10% formaldehyde, and processed for histology with hematoxylin and eosin (H&E) stain by Peking University Health Science Center. The histological micrographics were obtained through an Olympus BX51 microscope.

3. Results and discussion

3.1. Characterizations of GO with different lateral dimensions

It is gradually recognized that particle size should be well controlled [26–28], as broad size distributions often lead to ambiguous results in biological assessment. To obtain uniform-sized GO sheets, we used a rate separation method by making use of different sedimentation rates of graphene in certain size. AFM characterization (Fig. S1) showed that the resulting products were generally 350 nm and 2 μm in lateral dimension, and the average heights were 3.9 and 4.05 nm, respectively. Since the thickness of a single GO layer was about 1 nm [29], the minor difference in height (~0.15 nm) indicated identical layer amounts (≈4) of the two GO products. In addition, both of the sheets exhibited good colloid stability (Fig. S2) and equivalent surface carboxyl intensity (Fig. S3), which further assured the reproducibility and reliability of our subsequent evaluations.

3.2. Cytotoxicity assay of GO

To ensure the safety of nanomaterials before their entry into human application, *in vitro* toxicity should be considered upfront [30–32]. The typical method for GO preparation involves the employment of $KMnO_4$ oxidant, which unavoidably leads to heavy metal (Mn) contamination, raising our concerns about potential hazards of this carbon-material GO. To examine the cytotoxicity of metallic GO, a CCK8 assay was conducted after incubating cells with different treated GO (Mn-free and Mn-containing GO). As shown in Fig. 1A, significant toxicity was detected for all six kinds of cells that treated with Mn-containing GO. At a dose of 20 μg/mL, viability was even reduced by ~70% for HUVEC cells. Upon the removal of Mn, the GO in either lateral dimension had little effect on cell viability over present dose range (0–20 μg/mL). Besides CCK8 test, a LIVE/DEAD Cell Viability assay, which based on good esterase activity of live cells (indicated by calcein) and impaired membrane of dead cells (indicated by EthD-1), was also performed. As shown in the FACS plots, when macrophage PMØ (Fig. 1B) and non-phagocytic LLC (Fig. 1C) were exposed to Mn-free GO (10 μg/mL), they both emitted strong calcein signal (green) but little EthD-1 signal (red). In contrast, evident EthD-1 signal was detected in more than 40% PMØ cells and nearly 60% LLC cells after treating with Mn-containing GO at present lateral dimensions. These two cytotoxicity assays exhibited that the metallic GO could induce significant metabolic activity reduction as well as cell membrane injury, indicating an important consideration of potential toxic effect of GO without pretreatment. To ensure good cell viability, Mn-free GO were used in all subsequent experiments.

3.3. Size-independent cellular internalization of GO

Since biological performances of nanomaterial were highly related to the cellular uptake, we initially focused on evaluating the GO internalization in different cell types. Staining using a fluorescence probe was a conventional method to visualize nanomaterial in cells [33], whereas this was invalid for GO owing to its fluorescence quenching property [34]. To circumvent this obstacle, we exploited the photoluminescence property of GO in the near-infrared region (NIR). This property enabled us to directly quantify or visualize GO without fluorescence conjugation and preserved the original cell-GO structures. By using FACS technique, PE-Cy7 was tested to be an ideal channel for study of internalized GO, supporting the reported view that the GO was endowed with intrinsic fluorescence detectable through FL3 (with its set of wavelength filters similar to PE-Cy7) [35]. After exposure to 350 nm and 2 μm GO, HepG2, HKC, LLC, and HUVEC cells were examined on the PE-Cy7 channel (Fig. 2). Data showed that GO internalization was negligible in all these non-phagocytes (Fig. 2B), which was likely due to strong electrostatic repulsions between GO and cell surface (negatively charged). In our previous study, we demonstrated that although the cellular uptake of negative spherical particles was not as high as that of cationic or neutral particles, these particles could be internalized into non-phagocytic cells [36]. Distinct internalization capacity between the negatively charged GO and particles might be due to their different carboxyl distributions and curves. For the flat 2D GO, the curve was much smaller than that of spherical particles, imparting much higher carboxyl intensities when the cell-GO interaction happened. Therefore, the electrostatic repulsions between pristine GO and cell membrane would be more difficult to be conquered. From this point of view, when GO are used as drug carriers for these cells, functionalization including surface modification (*e.g.* receptor or peptide targeting) might be required for overcoming this repulsion. Contrary to little GO signal in non-phagocytic cells, obvious florescence increases were detected (Fig. 2A) in PMØ and J774A.1 cells, suggesting a high uptake capability of macrophages. Meanwhile, the FACS data showed an increase in side scatter (SS, indicating the inner complexity of the cells) in GO treated PMØ (Fig. S4), which was in agreement with the uptake behavior undergone by functionalized graphene in a recent study [13]. In addition, subsequent CLSM imaging (Fig. 2C and D) clearly exhibited the internalized 350 nm and 2 μm GO sheets in PMØ. Although the electrostatic repulsion still existed in the macrophage-GO interaction, the active phagocytosis might have been powerful enough to overcome this barrier, thereby resulting in great uptake capability. These results confirmed a dramatic uptake disparity between cell types and reflected the validity of our strategy to probe GO in cells.

Size effect has been reported to be responsible for the cellular internalization of conventional spherical or cylindrical particles [37–40]. Taking advantage of the probing method, we sought to

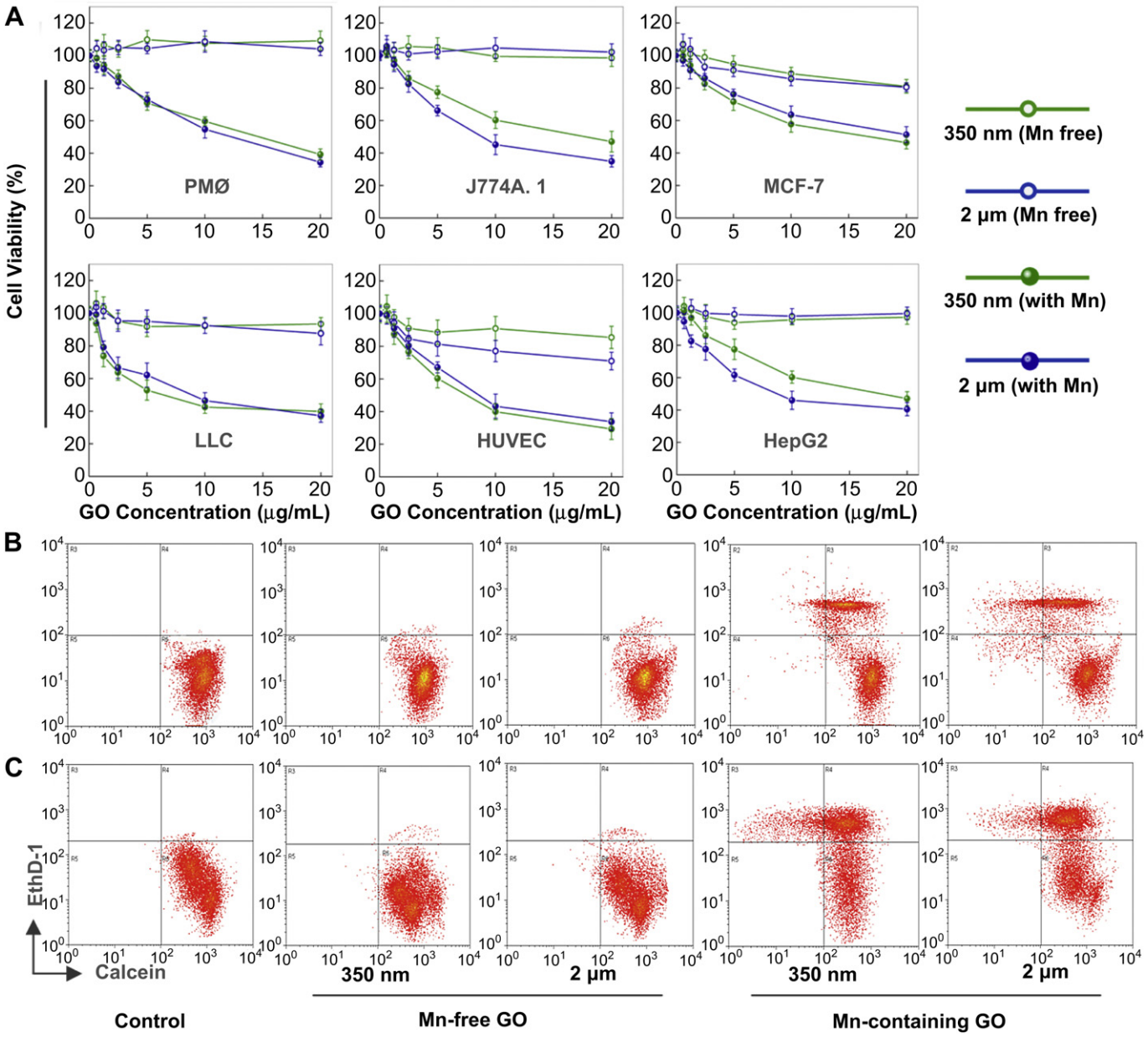

Fig. 1. Cytotoxicity assays of graphene oxide (GO) in macrophages and non-phagocytic cell lines, after 48 h incubation. (A) Cell-Counting Kit-8 assay showing the cytotoxicity events of GO in six cells. Each experiment was performed in triplicate, and data were represented as means ± standard deviation. (B and C) Live/Dead assay displaying the respective viability of peritoneal macrophages (PMØ) (B) and murine Lewis lung carcinoma (LLC) cells (C) at a GO concentration of 10 μg/mL. Negligible changes in viability were observed in all cells after exposure to pretreated GO (Mn-free), while dramatic decreases in viability were detected when cells were treated with Mn-containing GO, reflecting the potential hazard of using metallic GO in biological systems.

analyze the detailed internalization behavior of the two GO sheets in primary macrophages. Cellular internalization kinetics showed that the saturated uptake time was within 24 h (Fig. S5). Surprisingly, the saturated uptake amount of the two GO sheets did not vary with lateral dimension (Fig. 2B), and an identical accumulation of GO in macrophages was observed (Fig. 2C and D). It alluded that the GO were internalized into macrophages in a size-independent way that quite different from the conventional particles. In further support of this phenomenon, cells were exposed to GO over different doses (2 μg/mL to 6 μg/mL) (Fig. S6), and similar outcomes were obtained. The current observation, to the best of our knowledge, is the first revealed uptake profiles specific for this 2D material. This finding might open perspectives for controlling the biological response of materials through physics-derived solutions and facilitated the design of intelligent GO-based nanodevice on aspect of lateral dimension.

3.4. Cellular uptake mechanisms of GO in PMØ

To clarify why different size contributed equally to the final uptake amount of macrophages, we directed our interest into the mechanism of GO internalization. Aforementioned uptake inability of non-phagocytic cells suggested that the active phagocytosis might count most. Three major receptors are reported to be involved in phagocytosis: immunoglobulin G (IgG) Fcγ receptor (FcγR), complement receptor (CR), and mannose receptor (MR) [26]. Accordingly, the GO entry mechanism was determined by using specific inhibitors to block these three receptor-mediated

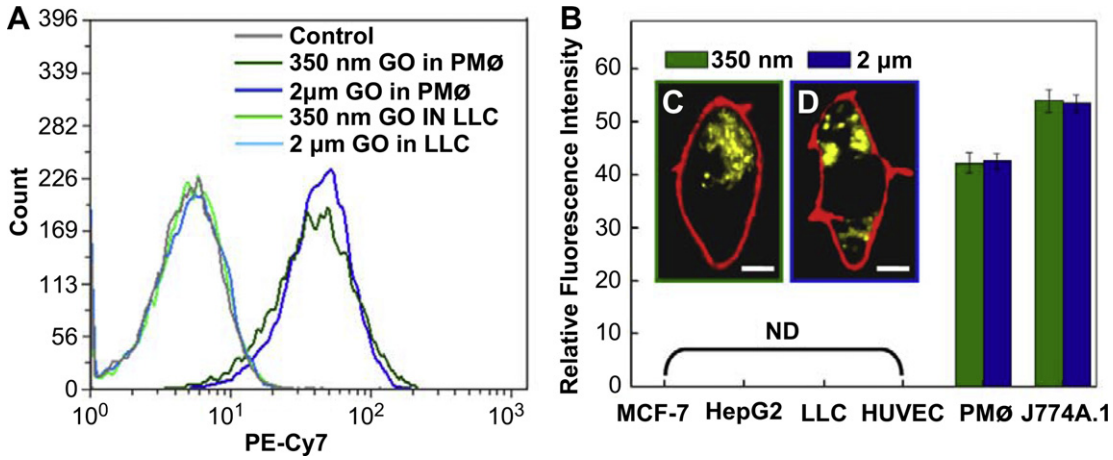

Fig. 2. Cellular internalization of GO in macrophages and non-phagocytic cells after 48 h incubation. (A) Flow cytometry (FACS) histogram exhibiting fluorescent signals from GO treated PMØ and LLC. (B) Data revealing the GO uptake capability of different cells. Each experiment was performed in triplicate, and data were represented as means ± standard deviation. (C and D) The inset laser scanning confocal microscopy (CLSM) showed the internalization of 350 nm (C) and 2 μm GO (D) by PMØ. Cell membranes were stained with Rhodamine-phalloidin (red), and the auto-fluorescent GO sheets were showed in yellow. Scale bars: 5 μm. (For interpretation of the references to color in this figure legend, the reader is referred to the web version of this article.)

pathways in macrophages. When MR- and CR-mediated phagocytosis were respectively blocked by anti-MR Ab and anti-CR Ab (or ethylenediaminetetraacetic acid) (Fig. 3A and Fig. S7), the cellular uptake of 350 nm and 2 μm GO was not altered, indicating a minimal contribution of these pathways in GO uptake by PMØ. In contrast, a significant uptake reduction was found after blocking the Fcγ receptor with IgG antibody, revealing a key role of the FcγR-mediated phagocytic pathway in GO entry. For further verification, we employed antibodies specific for the FcγR subtypes (FcγRI and FcγRIII). Again, obvious internalization decreases were detected for both antibody treatments, supporting the vital contribution of FcγR-mediated pathway in phagocytosing GO (Fig. S7). These results enlightened us a scheme to probe the phagocytosis mechanism for GO uptake (Fig. 3B) and an interpretation model for this size-independent event. As referred in the GO characterization, the 350 nm and 2 μm GO had a same layer amount (same height ≈4 nm), so the total surface area of the flat materials would be identical for different GO sheets with an equal quality amount. Accordingly, these two GO with same lateral area and surface properties could absorb equal amounts of IgG opsonin (Fig. S8). Interaction between the FcγR and IgG was proportional to the IgG absorption. Therefore, GO sheets differed greatly in size would be internalized by macrophages at a similar level through IgG-FcγR meditated phagocytosis.

To thoroughly delineate the GO internalization process, we tested the role of specific factors involved in macrophage uptake (Fig. 3C). The internalization of 350 nm and 2 μm GO was proved an energy-dependent process, as remarkable decreases (~85% compared with cells at 37 °C) occurred for GO under low-energy incubation (at 4 °C). In addition, the importance of actin remolding and microtubule movement of macrophages in response to exogenous GO was also verified. When cells were respectively treated with latrunculin B (Lat B) [41] and nocodazole (Noco) [42] to disrupt actin and microtubule movement, significant reductions of GO uptake were found. Moreover, corresponding CLSM images (Fig. 3D and E) exhibited prodigious morphology changes that undergone by PMØ upon contact with GO.

3.5. Cell-GO interaction before and after GO cellular entry

To date, there have been few studies reporting the initial contact and subsequent fate between cells and graphene. In the present work, we successfully captured detailed information during GO cellular uptake by using TEM technique (Fig. 4). Direct evidence of the cell-GO interaction images vividly showed the initial internalization process of GO. The 350 nm GO (Fig. 4A and B) were perceived and wrapped by the active filopodia of PMØ, in contrast, some 2 μm GO (Fig. 4E and F) were observed in an orientation near perpendicular to the plasma membrane intended for entry. In addition to the initial stage, the behavior of GO after internalization was also observed. Comparing with almost unvaried shape of 350 nm GO (Fig. 4C and D), obvious wrinkles were observed for accumulated 2 μm GO (Fig. 4G–I). This shape change involved two moves, owing to high steric effects undergone by the GO in microsize. The primary step was an oriented parallel wrinkle, as the lateral dimension of 2 μm was constricted to less than 300 nm (Fig. 4H). The secondary step was to form several zigzag folds based on the primary move (Fig. 4I). In comparison with almost no definite co-localization of lysosome for 350 nm GO (Fig. 4D), eligible lysosomal sequestration was found for some 2 μm GO (Fig. 4H). This phenomenon was further confirmed by CLSM imaging (Fig. S9). Although the mechanism remains unknown, such an inquiry into intracellular localization is of considerable importance for incorporating GO into components of biomedical devices. Exogenous substances are usually processed and degraded in endolysosomal compartments following internalization. The demonstrated non-lysosomal trafficking of GO, in principle, allows for delivering therapeutic peptides, proteins, or nucleic acid-based drugs to assigned organelles, while avoiding degradation in acid environment of lysosomes [43].

3.6. Inflammation-related response induced by GO

The above results illustrated the primary recognition and visible interaction of macrophages coming in contact with GO sheets. Following the internalization of exogenous substances, macrophages were prone to secrete numerous signaling molecules and trigger corresponding biological responses [44,45]. To investigate the subsequent immunological performances triggered by phagocytosis, a series of key cytokines, including IL-6, IL-10, IL-12, TNF-α, MCP-1, and IFN-γ, involved in inflammation were examined. Except for IL-10, fluorescence intensity signal (termed as PE-Log) of all cytokines significantly increased after 48 h in the 2 μm GO treated cells, comparing with weak improvement in the 350 nm GO treated

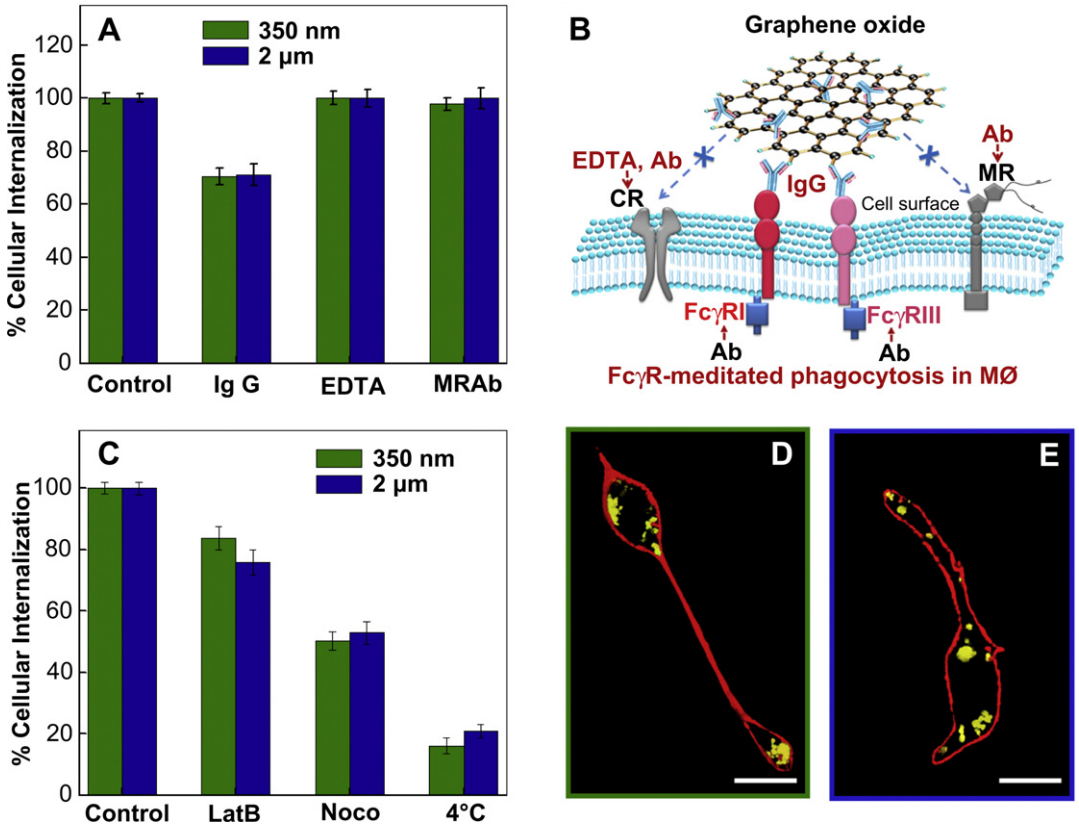

Fig. 3. Suggested receptor-mediated phagocytic mechanism and other important factors for GO uptake in PMØ. (A) GO internalization after blocking FcγR (IgG Fc receptor), CR (complement receptor), and MR (mannose receptor)-mediated phagocytosis. (B) Schematic histogram illustrating the phagocytic mechanism for GO entry in macrophages. (C) Histogram showing the role of filament/microtubule/energy-dependent factors in GO internalization. (D and E) CLSM images depicting morphology changes when PMØ came across 350 nm (D) and 2 μm (E) GO sheets. Scale bars: 10 μm. Each experiment was performed in triplicate, and data were represented as means ± standard deviation.

cells (Fig. 5A). Effects of incubation time (Fig. 5B and Fig. S10A) and GO dosage (Fig. 5C and Fig. S10B) were also examined. The inflammation cytokine secretion was found highly dependent on the GO dosage (Fig. 5C), particularly for the GO in micro-size. For example, when cells were incubated with 2 μm GO at the dose usage of 2, 4, 6 μg/mL, the resulted secretion level of IL-6 increased from 0.14 (for untreated cells) to 1.9, 7.0, and 20.0 ng/mL, respectively. However, the inflammation secretion arrived at a peak value at 48 h and then decreased as time prolonged. Recalling the detailed shape change during GO entry, we proposed that the high cytokine level induced by 2 μm GO might be attributed to the strong steric effect, which forced the micro-sized GO to strive for

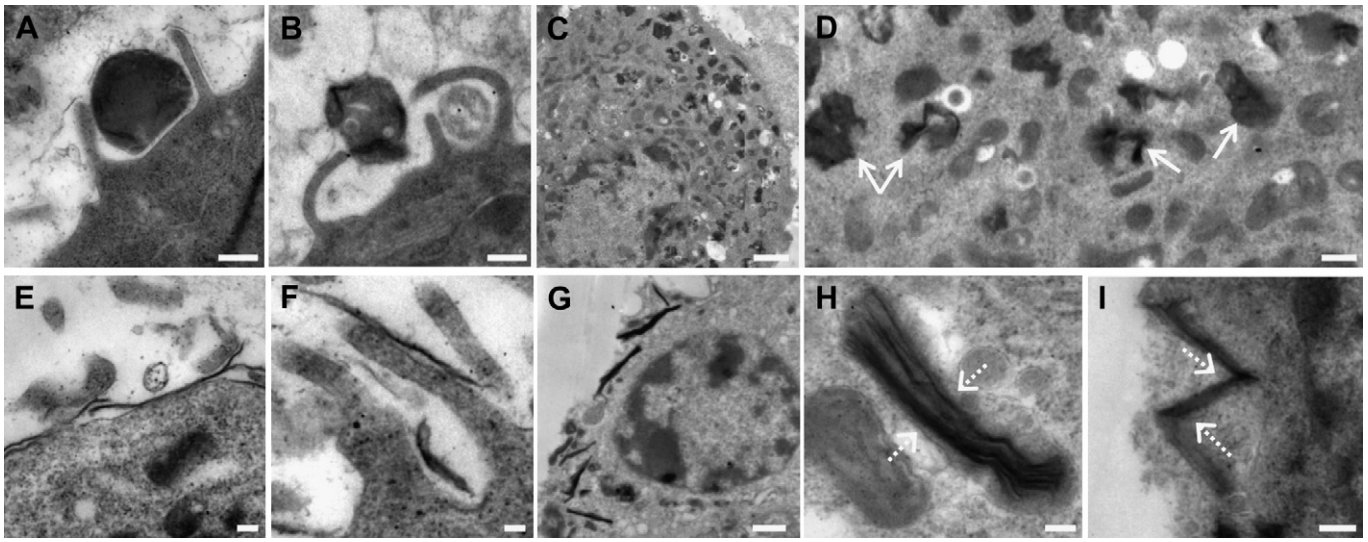

Fig. 4. Transmission electron microscopy (TEM) images illustrating the eligible internalization process of 350 nm (A–D) and 2 μm (E–I) GO sheets in PMØ. (A, B, E and F) TEM images of different GO interacting with cell membrane during initial cellular uptake. (C, D, G, H and I) Images showing the behavior of 350 nm GO (indicated by solid arrows) and 2 μm GO (indicated by dashed arrows) after being internalized. Scale bars: (C) and (G), 1 μm; others, 200 nm.

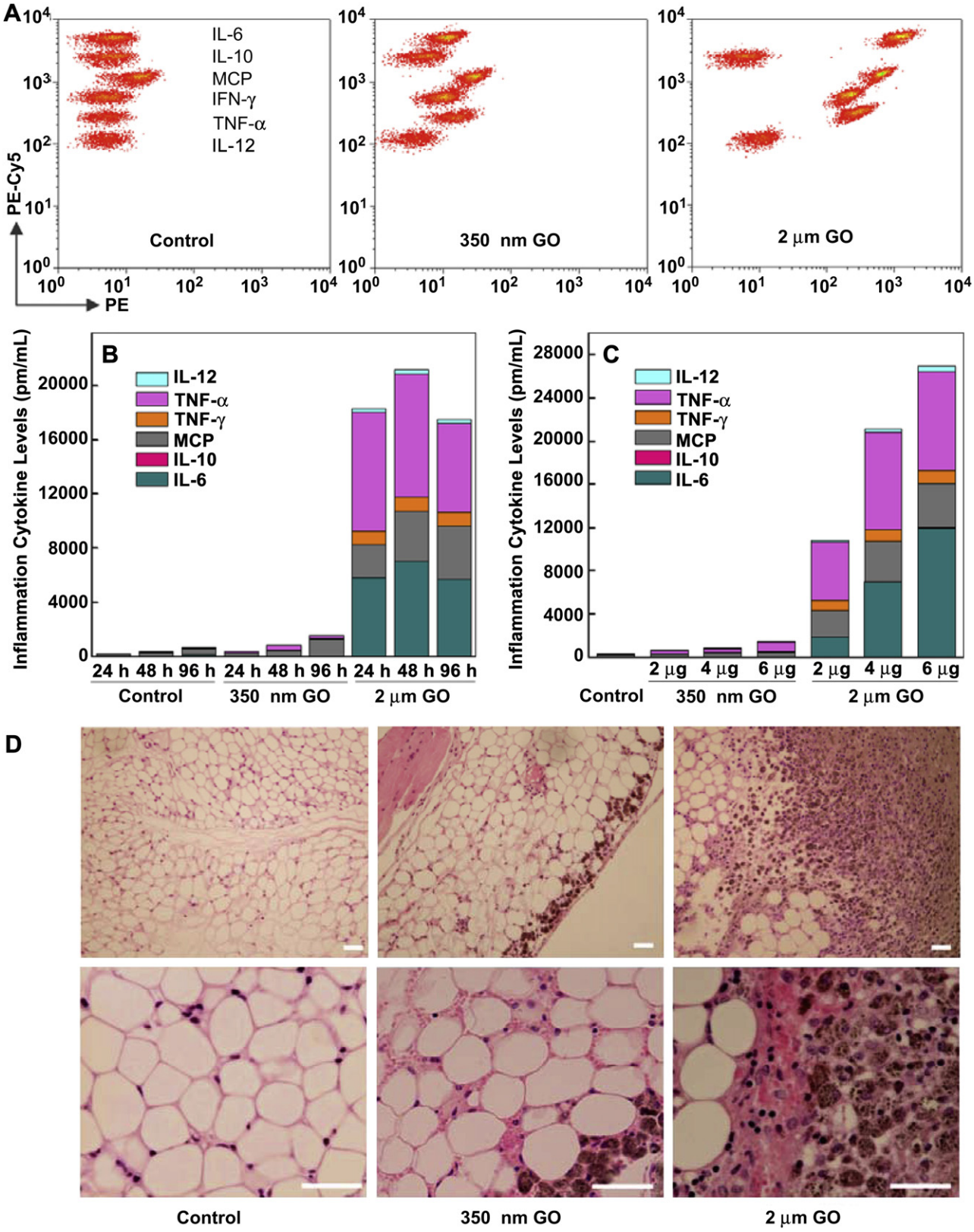

Fig. 5. Cytokine profile of PMØ after GO treatment. (A) FACS dot plots of cytokine expression determined *via* a CBA Mouse Inflammation kit. (B and C) Detailed cytokine production levels at different time points (B) or different GO dosage (C). (D) Histological micrographs displaying the migration of inflammation cells in C57/B6 mice after 21 days subcutaneous injection (s.c.) of GO. Scale bars: 50 μm.

a more stable state during the folding process inside the cells. This continuous struggle betrayed its extrinsic properties and thus resulted in recognition and fierce response from macrophages. As shown in Fig. 5D, when mice were injected subcutaneously with 2 μm GO, histological micrographics did indicate a strong inflammation response after 21 days. Comparing with regular normal fibrous tissue, a large number of mononuclear cells (such as macrophages and lymphocytes) infiltrated subcutaneous adipose tissue, and lipid-filled vacuoles as well as tissue impairment appeared after 2 μm GO-injection. In contrast, the inflammation response was weak under the treatment of 350 nm GO, only moderate cell filtration was observed. These results provided a deep understanding about the GO-cell interaction and fundamental views for the bio-application of GO. GO in micro-size may initially seem disappointing, since it is likely to induce an unexpected response or even inflammation-related diseases. However, highly upregulated cytokines are favored by adjuvants in vaccine system to activate the weak immune response. As for the GO in nano size, their much weak inflammation response is usually associated with good biocompatibility, which is favored for drug carrier and cancer therapy.

4. Conclusions

In summary, the cellular responses to GO sheets were systematically investigated, helping to fill an essential knowledge gap for developing GO in bio-applications. Enormous discrepancies were observed in different cell types, and the native GO were selectively internalized by the macrophages. Interestingly, the 2 μm and 350 nm GO greatly differed in size, but equally contributed to the uptake amount in macrophages. Similar amounts of antibody opsonization and active Fcγ receptor-mediated phagocytosis were demonstrated the cause of this behavior. In comparison with the size-independent uptake, the intracellular event and cytokine profiles were significantly regulated by lateral dimensions, and the GO in micro-size induced much stronger inflammation responses while nanosized graphene sheet showed better biocompatibility. While the present findings established some new concepts and proposed latent considerations for the bio-application of GO, the field is still in its infancy. In addition to study on lateral dimension effects, substantial work remains in exploring other physicochemical parameters (*e.g.* layer amounts and surface properties) of pristine GO or its functionalized derivatives. Detailed mechanisms of how relevant parameters affect the biological performance of GO also have to be elucidated case by case.

Acknowledgments

This work was supported by the 973 Program (2009CB930305), the National Nature Science Foundation of China (50703043) and Chinese Academy of Sciences (KGCX2-YW-210-1).

Appendix. Supplementary material

Supplementary data related to this article can be found online at doi:10.1016/j.biomaterials.2012.02.021.

References

[1] Zogovic NS, Nikolic NS, Vranjes-Djuric SD, Harhaji LM, Vucicevic LM, Janjetovic KD, et al. Opposite effects of nanocrystalline fullerene (C(60)) on tumour cell growth in vitro and in vivo and a possible role of immunosupression in the cancer-promoting activity of C(60). Biomaterials 2009;30:6940–6.
[2] Kam NWS, Liu ZA, Dai HJ. Carbon nanotubes as intracellular transporters for proteins and DNA: an investigation of the uptake mechanism and pathway. Angew Chem Int Edi 2006;45:577–81.
[3] Hirano S, Kanno S, Furuyama A. Multi-walled carbon nanotubes injure the plasma membrane of macrophages. Toxicol Appl Pharmacol 2008;232:244–51.
[4] Geim AK. Graphene: status and prospects. Science 2009;324:1530–4.
[5] Liu JB, Fu SH, Yuan B, Li YL, Deng ZX. Toward a universal "adhesive nanosheet" for the assembly of multiple nanoparticles based on a protein-induced reduction/decoration of graphene oxide. J Am Chem Soc 2010;132:7279–81.
[6] Rao CNR, Sood AK, Subrahmanyam KS, Govindaraj A. Graphene: the new two-dimensional nanomaterial. Angew Chem Int Ed 2009;48:7752–77.
[7] Yang XY, Zhang XY, Liu ZF, Ma YF, Huang Y, Chen Y. High-efficiency loading and controlled release of doxorubicin hydrochloride on graphene oxide. J Phys Chem C 2008;112:17554–8.
[8] Liu Z, Robinson JT, Sun XM, Dai HJ. PEGylated nanographene oxide for delivery of water-insoluble cancer drugs. J Am Chem Soc 2008;130:10876–7.
[9] Lu CH, Zhu CL, Li J, Liu JJ, Chen X, Yang HH. Using graphene to protect DNA from cleavage during cellular delivery. Chem Commun 2010;46:3116–8.
[10] Sun X, Liu Z, Welsher K, Robinson JT, Goodwin A, Zaric S, et al. Nano-graphene oxide for cellular imaging and drug delivery. Nano Res 2008;1:203–12.
[11] Feng L, Liu Z. Graphene in biomedicine: opportunities and challenges. Nanomedicine 2011;6:317–24.
[12] Liao KH, Lin YS, Macosko CW, Haynes CL. Cytotoxicity of graphene oxide and graphene in human erythrocytes and skin fibroblasts. Acs Appl Mater Inter 2011;3:2607–15.
[13] Sasidharan A, Panchakarla LS, Chandran P, Menon D, Nair S, Rao CNR, et al. Differential nano-bio interactions and toxicity effects of pristine versus functionalized graphene. Nanoscale 2011;3:2461–4.
[14] Singh SK, Singh MK, Nayak MK, Kumari S, Shrivastava S, Gracio JJA, et al. Thrombus inducing property of atomically thin graphene oxide sheets. Acs Nano 2011;5:4987–96.
[15] Yang XY, Wang YS, Huang X, Ma YF, Huang Y, Yang RC, et al. Multi-functionalized graphene oxide based anticancer drug-carrier with dual-targeting function and pH-sensitivity. J Mater Chem 2011;21:3448–54.
[16] Yang K, Zhang SA, Zhang GX, Sun XM, Lee ST, Liu ZA. Graphene in mice: ultrahigh in vivo tumor uptake and efficient photothermal therapy. Nano Lett 2010;10:3318–23.
[17] Ryoo SR, Kim YK, Kim MH, Min DH. Behaviors of NIH-3T3 fibroblasts on graphene/carbon nanotubes: proliferation, focal adhesion, and gene transfection studies. Acs Nano 2010;4:6587–98.
[18] Mitragotri S, Lahann J. Physical approaches to biomaterial design. Nat Mater 2009;8:15–23.
[19] Nel AE, Madler L, Velegol D, Xia T, Hoek EMV, Somasundaran P, et al. Understanding biophysicochemical interactions at the nano-bio interface. Nat Mater 2009;8:543–57.
[20] Yue ZG, Wei W, You ZX, Yang QZ, Yue H, Su ZG, et al. Iron oxide nanotubes for magnetically guided delivery and pH-activated release of insoluble anticancer drugs. Adv Funct Mater 2011;21:3446–53.
[21] Zhang YL, Guo L, Wei S, He YY, Xia H, Chen QD, et al. Direct imprinting of microcircuits on graphene oxides film by femtosecond laser reduction. Nano Today 2010;5:15–20.
[22] Hen J. Determination of surface carboxyl groups in styrene/itaconic acid copolymer latexes. J Colloid Interf Sci 1974;49:425–32.
[23] Major J, Fletcher JE, Hamilton TA. IL-4 pretreatment selectively enhances cytokine and chemokine production in lipopolysaccharide-stimulated mouse peritoneal macrophages. J Immunol 2002;168:2456–63.
[24] Weber TJ, Dutta D, Sundaram SK, Teeguarden JG, Riley BJ, Fifield LS, et al. Adsorbed proteins influence the biological activity and molecular targeting of nanomaterials. Toxicol Sci 2007;100:303–15.
[25] Simmet T, Lunov O, Syrovets T, Loos C, Beil J, Delecher M, et al. Differential uptake of functionalized polystyrene nanoparticles by human macrophages and a monocytic cell line. Acs Nano 2011;5:1657–69.
[26] Dobrovolskaia MA, McNeil SE. Immunological properties of engineered nanomaterials. Nat Nanotechnol 2007;2:469–78.
[27] Jiang W, Kim BY, Rutka JT, Chan WC. Nanoparticle-mediated cellular response is size-dependent. Nat Nanotechnol 2008;3:145–50.
[28] Lundqvist M, Stigler J, Elia G, Lynch I, Cedervall T, Dawson KA. Nanoparticle size and surface properties determine the protein corona with possible implications for biological impacts. Proc Natl Acad Sci USA 2008;105:14265–70.
[29] Stankovich S, Dikin DA, Dommett GHB, Kohlhaas KM, Zimney EJ, Stach EA, et al. Graphene-based composite materials. Nature 2006;442:282–6.
[30] Stone V, Johnston H, Schins RPF. Development of in vitro systems for nanotoxicology: methodological considerations. Crit Rev Toxicol 2009;39:613–26.
[31] Zhang Y, Ali SF, Dervishi E, Xu Y, Li Z, Casciano D, et al. Cytotoxicity effects of graphene and single-wall carbon nanotubes in neural phaeochromocytoma-derived PC12 cells. Acs Nano 2010;4:3181–6.
[32] Ge C, Du J, Zhao L, Wang L, Liu Y, Li D, et al. Binding of blood proteins to carbon nanotubes reduces cytotoxicity. Proc Natl Acad Sci USA 2011;108:16968–73.
[33] Sadik OA, Zhou AL, Kikandi S, Du N, Wang Q, Varner K. Sensors as tools for quantitation, nanotoxicity and nanomonitoring assessment of engineered nanomaterials. J Environ Monitor 2009;11:1782–800.
[34] Xie LM, Ling X, Fang Y, Zhang J, Liu ZF. Graphene as a substrate to suppress fluorescence in resonance Raman spectroscopy. J Am Chem Soc 2009;131:9890–1.
[35] Singh SK, Singh MK, Nayak MK, Kumari S, Gracio JJA, Dash D. Size distribution analysis and physical/fluorescence characterization of graphene oxide sheets by flow cytometry. Carbon 2011;49:684–92.

[36] Yue ZG, Wei W, Lv PP, Yue H, Wang LY, Su ZG, et al. Surface charge affects cellular uptake and intracellular trafficking of chitosan-based nanoparticles. Biomacromolecules 2011;12:2440–6.
[37] Yue H, Wei W, Yue ZG, Lv PP, Wang LY, Ma GH, et al. Particle size affects the cellular response in macrophages. Eur J Pharm Sci 2010;41:650–7.
[38] Shanbhag AS, Jacobs JJ, Black J, Galante JO, Glant TT. Macrophage/particle interactions: effect of size, composition and surface area. J Biomed Mater Res 1994;28:81–90.
[39] Gratton SE, Ropp PA, Pohlhaus PD, Luft JC, Madden VJ, Napier ME, et al. The effect of particle design on cellular internalization pathways. Proc Natl Acad Sci USA 2008;105:11613–8.
[40] Petros RA, DeSimone JM. Strategies in the design of nanoparticles for therapeutic applications. Nat Rev Drug Discov 2010;9:615–27.
[41] Geng Y, Dalhaimer P, Cai S, Tsai R, Tewari M, Minko T, et al. Shape effects of filaments versus spherical particles in flow and drug delivery. Nat Nanotechnol 2007;2:249–55.
[42] Bloom GS, Goldstein LS. Cruising along microtubule highways: how membranes move through the secretory pathway. J Cell Biol 1998;140:1277–80.
[43] De Koker S, De Geest BG, Singh SK, De Rycke R, Naessens T, Van Kooyk Y, et al. Polyelectrolyte microcapsules as antigen delivery vehicles to dendritic cells: uptake, processing, and cross-presentation of encapsulated antigens. Angew Chem Int Ed 2009;48:8485–9.
[44] Mantovani A. B cells and macrophages in cancer: yin and yang. Nat Med 2011; 17:285–6.
[45] Stow JL, Low PC, Offenhauser C, Sangermani D. Cytokine secretion in macrophages and other cells: pathways and mediators. Immunobiology 2009;214:601–12.